Role of resident electrons in the manifestation of a spin polarization memory effect in Mn delta-doped GaAs heterostructures

Mikhail V. Dorokhin [ORCID],[1] Mikhail V. Ved [ORCID],[1,*] Polina B. Demina,[1] Denis V. Khomitsky,[2] Kirill S. Kabaev,[2] Miguel A. G. Balanta,[3,4] Fernando Iikawa,[3] Boris N. Zvonkov,[1] and Natalia V. Dikareva[1]

[1]*Research Institute for Physics and Technology, Lobachevsky State University of Nizhni Novgorod, 603950 Nizhni Novgorod, Russia*
[2]*Department of Physics, Lobachevsky State University of Nizhni Novgorod, 603950 Nizhni Novgorod, Russia*
[3]*Instituto de Física "Gleb Wataghin," Universidade Estadual de Campinas, 13083–859 Campinas, SP, Brazil*
[4]*Universidade Federal de Uberlândia-ICENP, 38304-402 Ituiutaba, MG, Brazil*

The GaAs/InGaAs quantum wells with a ferromagnetic $\delta\langle Mn\rangle$ layer in GaAs barrier demonstrate a set of interesting spin-related phenomena originating from Mn-hole interaction. One of such phenomena is a spin-memory effect which consists of Mn spin polarization induced by interaction with vicinity spin-polarized holes generated under the exposure by short circularly polarized light pulses. Here long Mn spin relaxation time ($\sim$5 ns) allows preserving the spin polarization of the entire system. In the present paper the spin-memory effect investigation was carried out by analyzing the polarization kinetics of quantum-well photoluminescence in the pump-probe technique. It was shown that the photoluminescence circular polarization degree is strongly affected by the magnetic interaction of holes with Mn atoms prepolarized by the pump pulse. In the case of antiparallel Mn and hole polarizations, magnetic interaction leads to decrease of circular polarization degree as compared with single-pulse excitation (so called ΔP effect). Interestingly, the amplitude of hole-mediated ΔP effect is strongly affected by the concentration of resident electrons in the quantum well. The latter was shown to be caused by the specific compliance with selection rules for optical transitions with the participation of unpolarized resident electrons and spin-polarized holes affected by Mn-hole interaction.

I. INTRODUCTION

The influence of magnetic materials on the spin-dependent properties of light-emitting semiconductor structures is one of the central problems in spintronics and photonics, which if being properly solved may give rise to a number of promising applications in new generation of light-emitting devices (LEDs) [1–4]. One interesting manifestation of magnetic inclusions effect on LEDs operation is the interaction between spins of photogenerated carriers in the InGaAs/GaAs quantum-well (QW) heterostructures and a ferromagnetic manganese monolayer located in the immediate vicinity of the QW. A number of techniques was used to demonstrate that InGaAs quantum well provides circularly polarized photoluminescence (PL) emission upon the magnetization of ferromagnetic $\delta\langle Mn\rangle$ in GaAs [5–14]. The latter type of the generation of circularly polarized emission and corresponding spin polarization in InGaAs quantum well uses neither spin injection effect (see for example Ref. [2]) nor optical spin pumping (as in Ref. [15]) and thus is free of drawbacks attributive for each of the mentioned methods. The investigation of the exact mechanism of manganese magnetic effect on a spin polarization in a QW is a subject of interest which has been continuously explored within a decade [5–14]. Despite the long-term investigation, no general agreement has been reached on this matter yet. Earlier [7,8], it was supposed

that *p-d* exchange interaction between the Mn ions and holes in InGaAs quantum well leads to a spin polarization of the latter accompanied with a circular polarized emission. This supposition was disputed because of a large spatial separation between a QW and $\delta\langle Mn\rangle$ (up to 10 nm) exceeding the characteristic *p-d* interaction length for the holes. Moreover, a number of experiments studying the circular polarized PL dynamics were explained in terms of an electron spin polarization in the QW due to a spin-dependent escape from the quantum well to Mn-related defect states in the $\delta\langle Mn\rangle$ surrounding [9,10]. Some later experiments have provided new data disagreeing with the conclusions made in Refs. [9,10]. These are the inversion of circular polarization sign with the variation of Mn-QW spatial separation [12], and the increase of Larmor precession frequency upon magnetizing $\delta\langle Mn\rangle$ with circularly polarized light pulse [13,14]. Papers [12–14] have suggested the Mn interaction with holes in the quantum well; however, the exact interaction mechanism remains a subject of discussion and its analysis requires additional experimental data.

In the present paper we provide such kind of data concerning the magnetic interactions in InGaAs/GaAs/$\delta\langle Mn\rangle$ systems and specify some tools for efficient revealing of these interactions. To investigate the above system the pump-probe technique was applied. The pump pulse of circularly polarized laser emission was used to polarize Mn spins via the interaction with spin-polarized photoexcited holes [13]. The probe pulse with variable circular polarization was used to investigate the polarization state of Mn and the efficiency
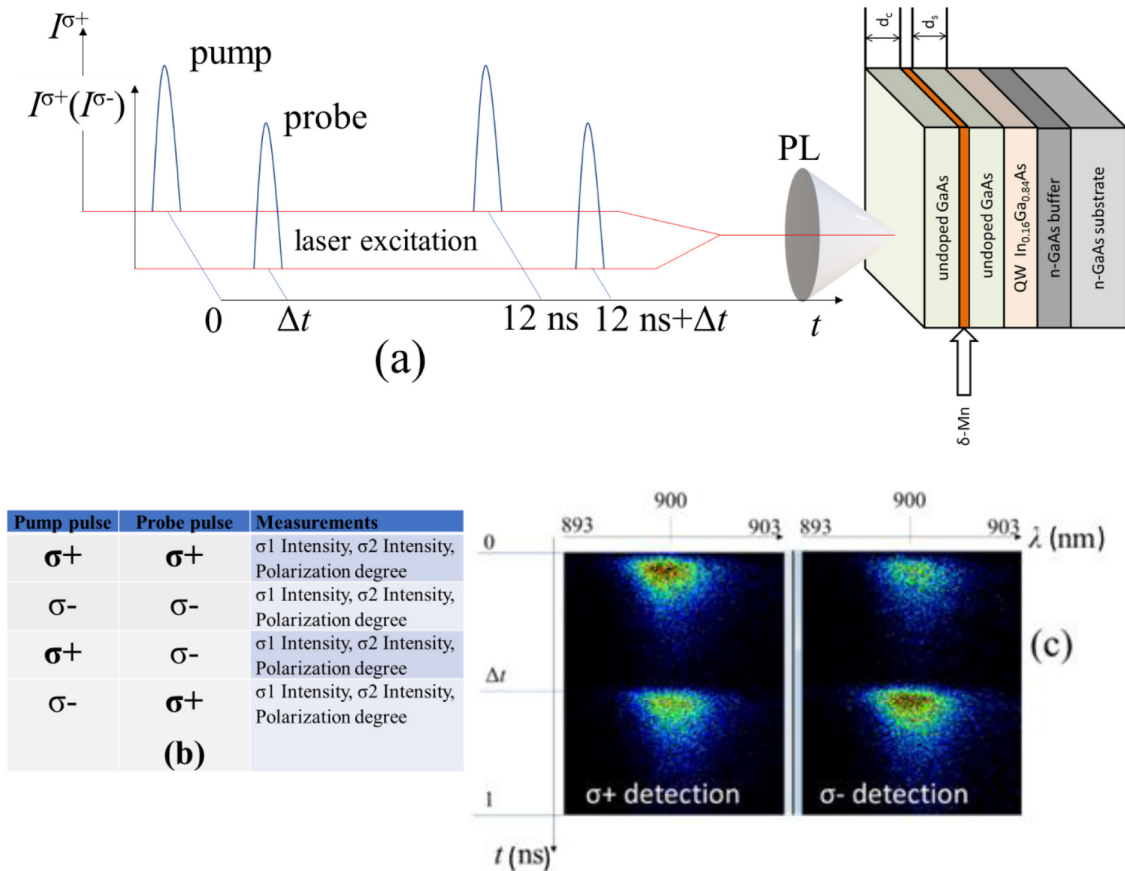
*mikhail28ved@gmail.com

FIG. 1. (a) The scheme of the sample excitation by pump and probe pulses shifted in time by Δt. The scheme of the investigated sample is shown at the right; (b) the scheme of sample excitation by laser pulses and detection. (c) Typical time-resolved PL results from sample No. 4 using two excitation beams with opposite circular polarizations. The time delay between the pulses is $\Delta t = 0.5$ ns, as shown by the schematic representation in (a). The streak-camera images correspond to the $\sigma+$ and $\sigma-$ components of the PL emission.

of Mn-hole interaction. The results obtained have shown that the resident electrons localized in the QW due to the donor doping of GaAs barrier play the dominating role in the observation of optical effects related with Mn-hole interaction. A generation-recombination balance model of the photoluminescence kinetics is derived; the model agrees with experimental data and confirms the role of resident electron concentration in obtaining the polarization dependencies in various samples.

II. EXPERIMENTAL DETAILS

The structures for investigation consisted of InGaAs quantum wells with a thin $\delta\langle Mn\rangle$ layer introduced into a GaAs barrier as shown in Fig. 1.

The variable technological parameter in batch under investigation was the spatial separation between InGaAs and $\delta\langle Mn\rangle$ (spacer layer thickness) which ranged between 2 and 8 nm. The samples were grown on n-GaAs (100) substrates using a hybrid system combining metal-organic chemical vapor deposition (MOCVD) and pulsed-laser ablation. First, n-GaAs buffer layer ($n \sim 2 \times 10^{16}$ cm^{-3}), the In$_{0.16}$Ga$_{0.84}$As quantum well (10 nm), and undoped GaAs spacer layer ($d_s = 2, 4, 6, 8$ nm) were grown by MOCVD at high temperature ($\sim 650\,^{\circ}$C). The precursors were trimethylgallium,

trimethylindium, and arsine; doping was carried out using laser sputtering of Si solid target [7]. On the second stage, we have used a Q-switched yttrium aluminum garnet: Nd laser ablation system with Mn and GaAs targets for growing the Mn delta-doping layer and the GaAs capping layer ($d_c = 40$ nm), respectively; the process temperature in this case was $400\,^{\circ}$C. The entire growth process was performed in the same reactor. Further details of the growth can be found in Refs. [7,8,12].

Time-resolved PL measurements were performed using a femtosecond Ti:Sa laser and a streak-camera system (time resolution $\sim$50 ps). The laser wavelength was tuned for resonant QW excitation. In the present paper the two-beam excitation scheme was used as in Ref. [13]. The pump circularly polarized beam was used to excite the system and a probe beam delayed by Δt was used for probing the resulting spin states in the structure. The right- ($\sigma+$) and left- ($\sigma-$) circular-polarized components of the excitation beams and the optical emission were selected with appropriated optics.

From now on we refer to the first pulses of the beam that arrive first and at a time of Δt prior to the second pulse as the pump pulses. Those that arrive at the time of Δt after the first pulse will be referred to as probe pulses. The results presented here correspond to the condition where the pump pulses are σ^+ polarized, and the following pulses from the second beam are σ^- polarized. Measurements with opposite polarizations
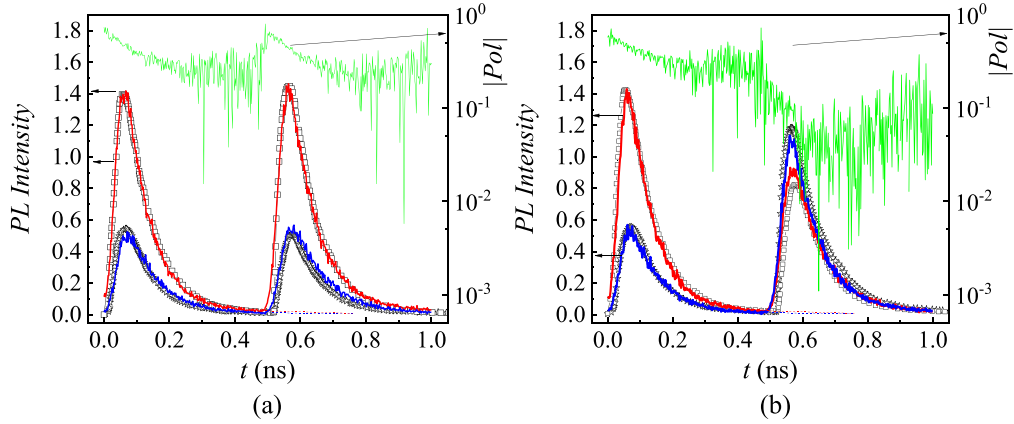
FIG. 2. Time dependencies of PL intensity (red and blue curves) and absolute values of circular polarization degree (green curve, raw curves without correction discussed in the text) calculated by (1), for sample No. 4 with $d_s = 8$ nm recorded in the modes of σ^+-σ^+ (a) and σ^+-σ^- (b) excitations at the temperature of 7 K. Red curves correspond to σ^+ circular polarization; blue curves correspond to σ^- circular polarization. The line+symbol plots show the intensities calculated using a spin-dependent generation-recombination kinetic balance model (discussed in Sec. III). The curves with squares correspond to calculated σ^+ polarized intensities; stars correspond to σ^- ones. Dashed curves, below the probe PL curves, show the estimated PL intensity from the pump pulse, using exponential decays, which are used to subtract from the probe PL intensity to correct the polarization degree due to the probe pulse.

were also performed and gave equivalent results. The degree of polarization of the PL emission is defined as

$$Pol = (I^{\sigma^+} - I^{\sigma^-})/(I^{\sigma^+} + I^{\sigma^-}), \quad (1)$$

where $I^{\sigma+/\sigma-}$ is the intensity of the $\sigma+/-$ emission component.

III. RESULTS AND DISCUSSION

The values obtained are in a good agreement with earlier results on similar samples with respect to a strong dependence of these parameters on a GaAs spacer layer thickness [13].

The probe pulse is either σ^+ or σ^- polarized and the polarization sign of corresponding PL emission follows the polarization of laser pulse. However, the absolute value of a polarization degree for σ^+-σ^- excitation case is significantly lower than that of σ^+-σ^+ excitation (the *Pol* value for the latter case is very close to pump emission polarization). The experimental *Pol* values at Fig. 2 (curves) are influenced by the pump-pulse emission.

If the polarization correction is performed (by subtracting the exponential decay of the first PL pulse from the intensity of the second one) [13] there is about 40% difference between *Pol* values for σ^+-σ^+ and σ^+-σ^- excitation cases. According to Ref. [13] such difference is due to effect of manganese polarization on the photogenerated carriers in the quantum well. The interaction of photoexcited spin-polarized holes with Mn leads to a spin polarization of the latter at the first stage of the process [13,14]. The characteristic interaction time is very short [14], and therefore cannot be revealed within our experimental techniques. However, Mn spin lifetime is rather long and thus it can influence the polarization dynamics even after the delay of Δt between pump and probe pulses.

Figure 3 shows the dynamics of the polarization difference value (ΔP) as

$$\Delta P(t) = \mathrm{abs}(|Pol^{\sigma^{+-}\sigma^+}(t)| - |Pol^{\sigma^{+-}\sigma^-}(t)|), \quad (2)$$

where $Pol^{\sigma^{+-}\sigma^+}$ is a polarization degree for σ^+-σ^+ excitation and $Pol^{\sigma^{+-}\sigma^-}$ is a polarization degree for σ^+-σ^- excitation scheme.

Since we have selected the σ^+ polarization of pump in both cases the ΔP value for the first PL pulse is zero with respect to experimental error. The probe laser pulse, on the contrary, is of different polarizations, which gives rise to nonzero values of ΔP for the second PL pulse. We note that there is only a short time period of rather high PL intensity during which ΔP value can be defined without a huge experimental error. As the intensity decreases the experimental error value raises significantly. For that reason, we will not discuss here the time dependence of ΔP and will focus on the values averaged over the time interval of $\sim$100 ps (when the high-PL intensity is preserved). Even with such limitation the ΔP is a very important parameter defining the behavior of the system.

The inset to Fig. 3 shows the temperature dependence of averaged value of ΔP effect (ΔP_a). At the temperature range
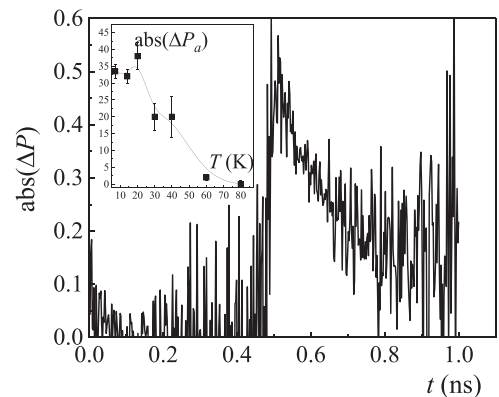

FIG. 3. Time dependence of ΔP value for sample No. 4 processed as in (2) at 7 K. The inset shows the temperature dependence of ΔP averaged over a time between 0.5 and 0.6 ns.
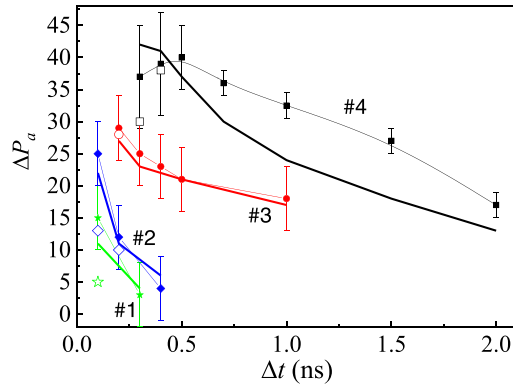
FIG. 4. The dependence of averaged ΔP on the delay time between two pulses (Δt) for all investigated samples. Solid dots correspond to experimental measurements; open dots correspond to the values calculated after subtracting the exponential decay of the first pulse from the intensity of the second one. Thick solid lines correspond to the ΔP_a values calculated using a kinetic balance model presented in Sec. III of the paper.

between 7–20 K the ΔP_a value does not change above the limits of an experimental error. Above 20 K a rapid decrease of ΔP is observed. However detectable ΔP effect was recorded even at 70 K which is above the Curie temperature of $\delta\langle Mn\rangle$ (30–40 K) [7,8].

Figure 4 shows the dependence of ΔP on the delay time, Δt, for all investigated samples.

With the increase of the delay the values ΔP_a decrease which should take place due to a spin relaxation of Mn. The Mn spin-relaxation time is about 5 ns (estimated by the model discussed below), which although rather high yet can be visualized within the explored time windows. The ΔP_a decrease for small delays for the sample No. 4 cannot be unambiguously confirmed because of the huge experimental errors arising from the necessity to subtract the intensity decays from the first pulse. Taking the experimental error into account we can only state that ΔP does not change significantly for the Δt range from 300 to 500 ps. The characteristic decay time of the ΔP effect can be estimated for samples No. 3 and No. 4 as approximately 5 ns. For the samples No. 1 and No. 2 this value cannot be estimated due to a relatively big experimental error and small initial value of the effect. The most surprising result is a decrease of ΔP_a value with the decrease of the spatial separation between $\delta\langle Mn\rangle$ and a quantum well. Indeed, the amplitude of various Mn-hole interaction effects usually increases as d_s decreases [6–12]. Nevertheless, the greatest ΔP effect was detected for the sample with the highest d_s among the entire set. The latter result does not agree with the one obtained in Ref. [13] for similar samples; the reason for such a disagreement will be discussed in the next section of the paper.

IV. KINETIC BALANCE MODEL

Let us now switch to a discussion of the experimental results. First, we will briefly discuss the qualitative model of dynamic spin polarization in the investigated samples; then,
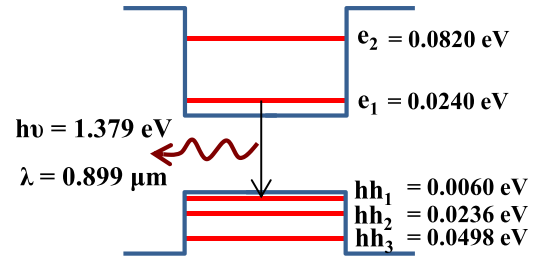

FIG. 5. Calculated energy-band diagram of strained In$_{0.16}$Ga$_{0.84}$As 10-nm-wide quantum well using the software developed in Refs. [16,17].

we will present the results of theoretical calculations which were performed by solving the balance equations.

The consideration below is based on the calculations of energy band diagram of strained In$_{0.16}$Ga$_{0.84}$As 10-nm-wide quantum well using the software developed in Refs. [16,17] and on the conclusions firstly made in Refs. [13,14]. A calculated system of energy levels in a strained quantum well with enclosed $\delta\langle Mn\rangle$ layer is shown in Fig. 5. A system includes three heavy-hole levels and two electron levels. Because of the compression strain the light holes are pushed away from the QW [16,17] and do not contribute to the polarization dynamics.

Due to resonant excitation conditions in our experiment, only e_1-hh_1 transition was excited. The carrier thermal escape to the higher levels is insignificant due to a low measurement temperature. This allows us to take into account only one electron and one heavy hole level as is schematically shown in Fig. 6.

Second, the distinguishing feature of our system is that GaAs substrate and the buffer layer are donor doped (unlike Ref. [13]). Since Mn is an acceptor impurity, the quantum well is located between the n-GaAs and p-(Ga,Mn)As layers, i.e., in a space-charge region of p-n junction. The type and concentration of carriers in the quantum well thus depend on its position relative to the boundaries of the p- and n regions [18,19]. We assume that in a steady-state condition, conduction electrons from the n-GaAs buffer layer are localized in a QW. The greater the separation between the QW and delta layer, the higher is the concentration of these "resident" electrons. For the sample No. 4 with $d_s = 8$ nm, the electron concentration in the QW is maximum among all structures, and for sample No. 1 with $d_s = 2$ nm, it is minimum (close to zero).

Third, various spin-relaxation mechanisms can be of interest for different subsystems of our structure, including the electrons, holes, and Mn spins. In particular, the Mn spin relaxation may depend on several interaction mechanisms including the Dzyaloshinskii-Moriya exchange. We utilize the spin-relaxation mechanisms in the model in a form of typical relaxation parameters without studying their microscopic origin which is a challenging and fruitful task but is out of the scope of the present paper.

Finally, we neglect the effects of nuclear spin polarization, although they can in principle modify the level structure due to the hyperfine interaction. However, the typical level shifts in GaAs or InAs structures are about 10 μeV for electrons
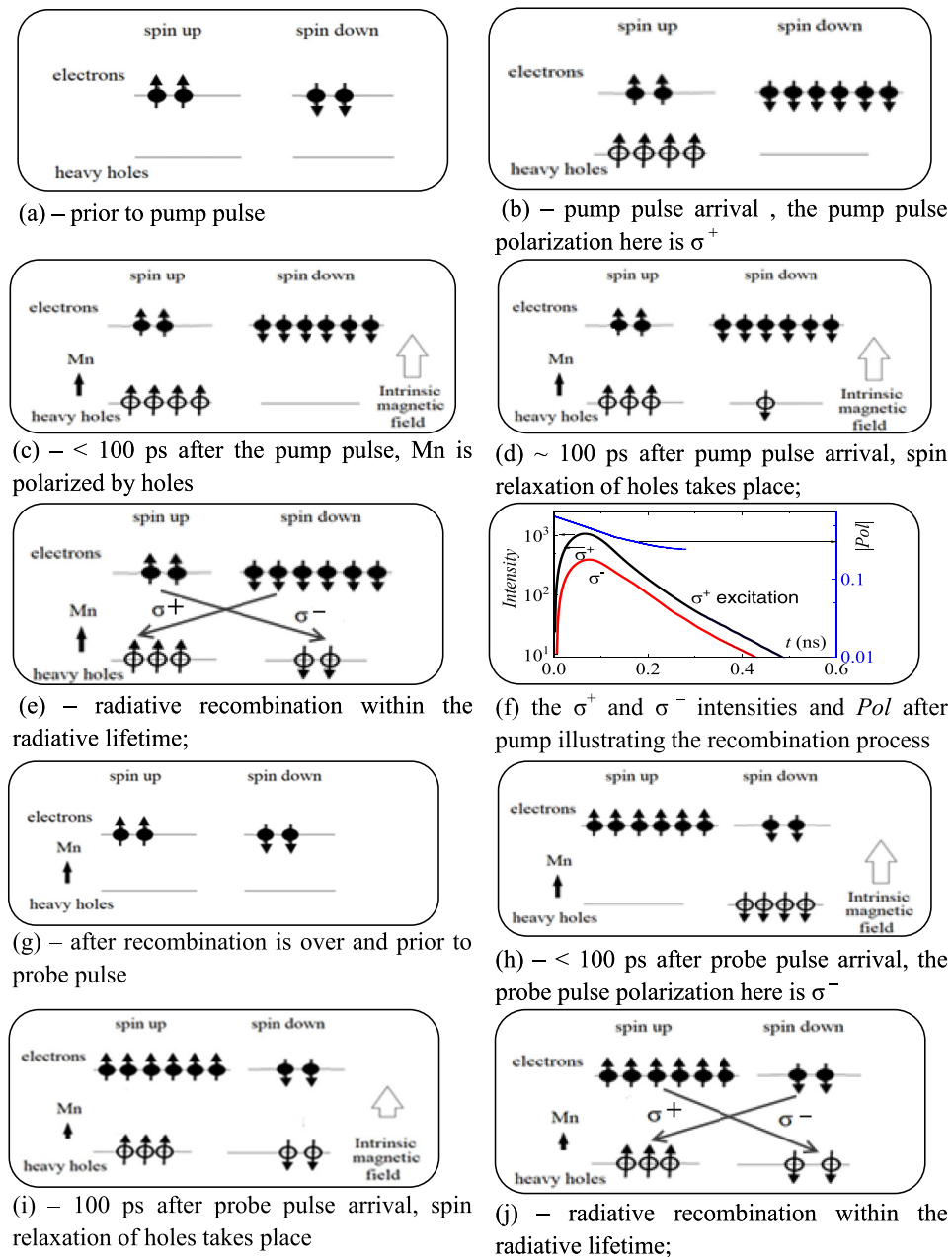
FIG. 6. Scheme of filling of energy levels in the strained quantum wells with respect to polarization, carrier generation by pump and probe pulses, and recombination. The small arrows show the spins of a different sign. The big arrow represents the effective magnetic field acting on holes.

and 1 μeV for holes [20]. Since the spectral beam width of our laser pulse is by an order of magnitude greater, such shifts seem to be out of big significance.

Now we turn to the step-by-step description of the excitation and relaxation processes described below by the kinetic balance model.

(i) Prior to the circularly polarized pump-pulse arrival (i.e., without any external fields) the polarization of resident electrons is zero, i.e., the concentrations of resident electrons with the spins of $+1/2$ and $-1/2$ are equal [Fig. 6(a)].

(ii) As a pump pulse arrives the electron-hole pairs are generated in the QW, as is shown in Fig. 6(b). The photoexcited holes and electrons are spin polarized with respect to

selection rules. Due to a resonant excitation the initial spin polarization of photoexcited electrons and holes is close to 100% as is shown in the diagram, and the spin-relaxation effects are not considered yet. The polarized photoexcited electrons with the concentration of N are added to unpolarized resident electrons in the QW.

(iii) Within the time of less than 100 ps the spin orientation of Mn ions occurs due to interaction with holes [Fig. 6(c)]. This process and its characteristic timescale were experimentally confirmed for similar systems in Refs. [13,14].

(iv) Within the time of about 100 ps fast-hole spin-relaxation process provides the redistribution of heavy-hole spins into some equilibrium state (fast-hole spin relaxation

is in agreement with earlier works, e.g., Refs. [9,14,21]). We note that in general 3/2 spin and −3/2 spin concentrations are not equal to one another due to a Mn spin polarization influence on heavy holes [Fig. 6(d)].

(v) At the next stage, the radiative recombination of spin-polarized photoexcited carriers starts to play a role in electron-hole dynamics [Figs. 6(e) and 6(f)]. Radiative transitions proceed in accordance with the selection rules and taking into account the spin polarization of electrons and holes. Since each of the spin states in a system is filled with electrons and holes (with different concentrations though), the degree of polarization is less than unity. We note that the value of *Pol* ∼ 0.7 at the start of emission process is another experimental evidence of the resident electrons' presence in the quantum well.

The value of *Pol* is determined by the spin polarization of electrons and holes. As the radiative recombination proceeds, spin relaxation of electrons takes place; as a result, circular polarization degree decreases with time. The spin-relaxation time of electrons and the radiative lifetime differ by about the order of magnitude; however, the processes of recombination and spin relaxation of electrons are clearly visible in the recombination dynamics.

(vi) Prior to a probe-pulse arrival, the carrier distribution between the energy levels is similar to the one shown in Fig. 6(a) with the only exception of Mn being spin polarized since the Mn spin decaying time is greater than the delay times used [14]. The QW levels are filled with equilibrium electrons with equal or nearly equal concentrations of +1/2 and −1/2 spins (Fig. 6(g)].

(vii) When the probe-pulse polarization is σ^- the spin polarization of photoexcited carriers is inverse to the one shown in Fig. 6(b) [Fig. 6(h)]. Next process is a Mn polarization due to interaction with spin-polarized photoexcited holes. Unlike the pump-pulse situation [shown in Fig. 6(d)], by the time of probe-pulse arrival the Mn is spin polarized in the opposite direction. The pump pulse in this case should decrease the absolute value of Mn spin polarization, whereas the sign of Mn spin may vary depending on the strength of Mn-hole interaction. Both of the cases provide changes in hole spin-relaxation process as compared with the one shown in Fig. 6(d). In Fig. 6(i) we have shown the case of Mn spin being the same sign as after the pump pulse but smaller in polarization degree. In this case hole spin relaxation in the presence of Mn-hole interaction should lead to a small "negative" spin polarization of holes.

(viii) As a result, the spin-dependent radiative recombination conditions change. The PL polarization in this case is a result of competition between the minority and majority carrier spin transition shown in Fig. 6(j). Without considering the Mn spin polarization, now the $\sigma-$ transition should be dominant, due to the configuration shown in Fig. 6(h). However, such redistribution of the holes due to the Mn-hole interaction leads to another PL polarization [Fig. 6(i)], decreasing the circular polarization degree in absolute value [as observed in Fig. 2(b)]. This decrease should be dependent on the spatial separation between the Mn atoms and the holes in the QW. But, we observed that it also depends on the density of the resident electrons in the QW, as will be discussed later. This is due to the $\sigma+$ transition being dependent on

the density of the electrons in the spin-down states, as shown in Fig. 6(j).

In the samples with higher concentration of resident electrons, the spin-down electron recombination intensity is also higher and the polarization degree becomes smaller. This explains the "inverse" dependence of the spin-memory ΔP effect on the thickness of the spacer layer. With a large thickness of spacer GaAs, the concentration of resident electrons is the highest, which makes the maximum contribution to the intensity of "minority" polarized PL and, accordingly, decreases the overall circular polarization degree. As the thickness of the spacer layer decreases, the concentration of resident electrons decreases, thus decreasing the number of recombination events with a minority spin. The efficiency of the interaction between the spins of holes and manganese in the structures under study plays a secondary role. According to the numerous experimental data [12,18], the efficiency of interaction between Mn and holes weakly depends on the thickness of the GaAs spacer layer.

A. Modeling

The above processes were modeled via the time-dependent spin-resolved equations describing hole and electron generation by laser pulses, the interaction of holes with *Mn* ions in the delta layer, and the carrier recombination with emission of the circular polarized photons [13]. They include the electron concentrations $N_{1,2}^e(t)$ with spin −1/2 or +1/2, respectively, the heavy-hole concentrations $N_{1,2}^h(t)$ with spin $\mp 3/2$, and the *Mn* ion concentrations $N_{1,2}^{Mn}(t)$, which gives in total six components and the corresponding system of six balance equations governing the evolution of the concentrations [22,23].

The change in concentrations of spin-polarized electrons, holes, and Mn follows the balance equations:

$$\frac{dN_{1,2}^e}{dt} = A\boldsymbol{\sigma}_{2,1}(t) - B \cdot \min\{N_{1,2}^e, N_{2,1}^h\} - \boldsymbol{\gamma}_e \Delta N_{1,2}^e$$

$$\frac{dN_{1,2}^h}{dt} = A\boldsymbol{\sigma}_{1,2}(t) + C \cdot f(N_{1,2}^h) \cdot \Delta N_{1,2}^{Mn}$$
$$- B \cdot \min\{N_{2,1}^e, N_{1,2}^h\} - \boldsymbol{\gamma}_h \Delta N_{1,2}^h$$

$$\frac{dN_{1,2}^{Mn}}{dt} = D \cdot f(N_{1,2}^{Mn}) \cdot \Delta N_{1,2}^h - \boldsymbol{\gamma}_{Mn} \Delta N_{1,2}^{Mn}. \qquad (3)$$

The electrons and holes may be created with the absorption of incident photons, and annihilated with the emission of photons having the polarization depending on the electron and hole spin projections. The first two terms of Eq. (3) $[A\boldsymbol{\sigma}_{2,1}(t)]$ refer to the generation of electron-hole pairs by the laser pulses $\sigma_{2,1}(t)$ referring to σ^+ and σ^- circular polarizations, correspondingly. The laser pulses have a sharp delta-shaped profile with a width of $\tau_p \sim 0.1$ ps, much shorter than streak-camera resolution, ∼50 ps, and are delayed from one another by the window Δt ranging from 300 to 2000 ps. Besides the generating terms stemming from the laser pulses, the balance equations for electrons and holes include the annihilation terms describing the photoluminescence proportional to the minimum of the concentrations for the two participating components ($B \cdot \min\{N_{i,j}^e, N_{j,i}^h\}$, $i, j = 1, 2$). These terms take

into account the selection rules for optical transitions in the quantum well.

The third group of terms describes the interaction between the holes and the spins in the *Mn* layer. These two phenomenological terms depend on the hole and *Mn* polarization (actually, depend on the difference between hole and *Mn* spin concentrations); they can be introduced as $C \cdot f(N_{1,2}^h) \cdot \Delta N_1^{Mn}$ for holes and $D \cdot f(N_{1,2}^{Mn}) \cdot \Delta N_{1,2}^h$ for Mn in the second and third pairs of Eq. (3) respectively. Here C, D are Mn-hole interaction constants. The function $f(N_{1,2}^h)$ describes the spin channel from which the hole spins can be taken for increasing the corresponding spin population. Consider $\frac{dN_1^h}{dt}$; the change in N_1^h is only possible when there is $N_2^h \neq 0$. In this case $f(N_{1,2}^h) = N_2^h$ and the entire term for Mn-hole interaction is $\frac{dN_1^h}{dt}(Mn-hole) = C \cdot N_2^h \cdot \Delta N_1^{Mn}$. Similar function $f(N_{1,2}^{Mn})$ is present in the balance equation for *Mn* spins. The concentration dependencies of $f(N_{1,2}^h)$ and $f(N_{1,2}^{Mn})$ create a nonlinearity in the system (3) so it is necessary to use numerical methods for solving it. Then, from (3) the conservation of the total *Mn* concentration $(N_1^{Mn} + N_2^{Mn})$ follows since $d(N_1^{Mn} + N_2^{Mn})/dt = 0$, while the hole and electron concentrations are not conserved due to the laser pulse generation and subsequent photoluminescence.

The final group of terms in all equations describes spin relaxation with characteristic rates γ_e, γ_h, and γ_{Mn} for the electrons, the holes, and *Mn* spins, respectively. The relaxation terms are proportional to the corresponding differences in spin-resolved concentrations $\Delta N_{1,2}^e$, $\Delta N_{1,2}^h$, and $\Delta N_{1,2}^{Mn}$. Here for brevity, we define $\Delta N_1^e = N_1^e - N_2^e$, $\Delta N_2^e = N_2^e - N_1^e = -\Delta N_1^e$, and so on.

The relaxations rates in Eq. (3) are taken from the tables of corresponding material parameters while the constants *A*, *B*, *C*, and *D* are mainly fitting parameters determined from the experimental data on the photoluminescence. The set of equations in (3) is accompanied by the initial conditions where we set the total concentration of *Mn* spins interacting with holes to *1* as a unit for nondimensional concentrations so $N_1^{Mn}(0) = N_2^{Mn}(0) = 1/2$, and express the initial nonzero electron concentrations via this unit. The initial hole concentration in our samples is zero.

When the spin-resolved concentrations are found as a solution of system (3), one can write the circular photoluminescence intensities (I_{01} is the left polarization and I_{02} is the right polarization):

$$I^{\sigma+} = B\min\{N_2^e, N_1^h\}$$
$$I^{\sigma-} = B\min\{N_1^e, N_2^h\}. \tag{4}$$

After obtaining the intensities one gets also the polarization degree defined by (1). The time dependencies of the recorded intensities (4) and the polarization (1) will be the subject of our interest in the following section for two cases of laser pulse:

Parallel case 1: σ^+ pulse followed after window Δt by the same σ^+ pulse;

Antiparallel case 2: σ^+ pulse followed after window Δt by the oppositely polarized σ^- pulse.

Following Sec. II, the polarization (1) for each pulse sequence is labeled as *Pol*^p (parallel) and *Pol*^a (antiparallel)

TABLE I. The dynamic parameters obtained from the fitting of the experiment results of PL intensity and polarization degree decays based on the model discussed in Sec. III.

Sample No.	d_s (nm)	PL decay time τ (ps)	Electron spin lifetime $1/\gamma_e$ (ps)
1	2	22 ± 5	230 ± 20
2	4	46 ± 5	160 ± 20
3	6	65 ± 5	270 ± 20
4	8	85 ± 5	670 ± 20

and the corresponding polarization module difference ΔP is defined by (2). The value of ΔP reflects the influence of the holes and the *Mn* layer. The long spin-relaxation time for *Mn* creates a "spin-memory effect" which shifts the hole spin polarization following the sign of *Mn* spin polarization, leading to the decrease in the absolute value of polarization (1) after the second laser pulse.

One other thing to notice considering the investigated system is the equality of polarizations after first and second pulse of the same polarity [Fig. 2(a)] which provides a very important condition of Mn polarization by the laser pulse. We believe that the holes generated by the pump laser pulse provide near 100% spin polarization of interacting Mn atoms and hence the probe laser pulse of the same polarity does not lead to a significant change in Mn polarization. On the contrary, the probe laser pulse of inverse polarity can lead to reorientation of Mn spins. See Table I.

B. Results of modeling

We consider the following parameters for the sample No. 4 where the maximum polarization difference has been achieved.

(i) The initial concentrations $N_1^{Mn}(0) = N_2^{Mn}(0) = 1/2$; we choose N^{Mn} as a reference unit of concentration. The resident electron concentration is $N_1^e(0) = N_2^e(0) = 2.26 \times 10^{-4}$, which has been estimated from the band picture of the system at 10 K. The resident hole concentration is zero $[N_1^h(0) = N_2^h(0) = 0]$, since these conditions should provide the dependence shown in Fig. 3.

(ii) The relaxation rates in units of 1/ps are $\gamma_e = 1.493 \times 10^{-3}$ 1/ps and $\gamma_h = 0.027$ 1/ps, as has been evaluated earlier for the similar systems [14]. From the photoluminescence experiments presented in Ref. [14] we get $\gamma_{Mn} = 2.0 \times 10^{-4}$ 1/ps.

(iii) The remaining parameters $A = 0.0128$ 1/ps and $B = 0.0125$ 1/ps define the generation and photoluminescence rates. The parameter B is defined via the experimentally measured photoluminescence data and is sample dependent while the generation rate is assumed to be constant for all samples. The parameters C and D should be for the best fit to the experimental data. Being multiplied by the hole and Mn spin-resolved concentrations $N_{1,2}^h$ and $N_{1,2}^{Mn}$ they define in system (3) the polarizations rates for hole and Mn spins due to interaction with each other. For the given experimental conditions maximal achievable hole concentration (in units of Mn spins) reaches the value $N_{1,2 \max}^h = 0.0013$ for all samples, while $N_{1,2 \max}^{Mn} = 1$.

TABLE II. The values of preset and fitting parameters for Eq. (3).

Sample	1 ($d_s = 2$ nm)	2 ($d_s = 4$ nm)	3 ($d_s = 6$ nm)	4 ($d_s = 8$ nm)
A – hole and electron generation rate (1/ps)	0.012 8	0.012 8	0.012 8	0.012 8
B – radiative recombination rate (1/ps)	0.045 4	0.021 2	0.016 1	0.012 5
$C \cdot f(N_{1,2\,max}^h)$ – rate of hole polarization by Mn (1/ps)	0.044	0.044	0.044	0.044
$D \cdot f(N_{1,2\,max}^{Mn})$ – rate of Mn polarization by holes (1/ps)	0.032 5	0.032 5	0.032 5	0.032 5
γ_e (1/ps)	0.004 348	0.005 882	0.003 703	0.001 493
γ_h (1/ps)	0.027	0.027	0.027	0.027
γ_{Mn} (1/ps)	0.000 2	0.000 2	0.000 2	0.000 2

The results of modeling for the recorded intensities (3) are shown in Fig. 2 for $\Delta t = 500$ ps. The streak camera has a finite time resolution defined as a convolution window Δt_c which is about 50 ps in our experiments. For that reason, calculated intensities were expressed via the camera convolution kernel $K(t-\tau)$ in the Gaussian convolution form. With the detector convolution function taken into account there is a good agreement between experimentally measured and calculated PL curves upon the solution of equations in system (3). This proves that the experimentally revealed behavior of QW/$\delta\langle$Mn$\rangle$ system can be adequately explained within our model.

Another important parameter is the total concentration of Mn spins $N_1^{Mn} + N_2^{Mn}$ actively interacting with holes and serving as a unit of concentration. It is a natural suggestion that this number is sample dependent since the distance d between the Mn layer and the holes in QW is varied. The greater is d, the smaller fraction $N(d)$ of Mn spins is expected to interact efficiently. If we expect a tunnel-like overlap of Mn and hole wave functions, then an exponential fit of the present form may be considered:

$$N(d) = N(d_0) \exp\left(-\frac{d - d_0}{d_0}\right), \qquad (5)$$

where d_0 and $N(d_0)$ are the reference distance and concentrations which we take for the sample No. 4 with $d = 8$ nm. The values of both preset and fitting parameters for Eq. (3) are listed in Table II for all sets of samples. It should be noted that for setting the initial electron concentration values in the last line of Table II we take into account the experimentally obtained absolute values of the resident electron concentration as well as the scaling function (5).

The calculation procedure performed for the sample No. 4 with $\Delta t = 500$ ps was first repeated for different delay times and theoretical dependence of ΔP_a vs Δt was plotted (Fig. 3, thick lines). We believe that the parameters of the equation discussed above are fundamental characteristics of system behavior and therefore should not change with a change in the delay time. For that reason, we have used all the same modeling parameters as in the 500-ps case. However, the change in the sample structure, in particular the spacer layer thickness, might deviate some of the Eq. (3) parameters discussed in the previous section. For that reason, when performing the same calculation procedure for the rest of the batch one should renormalize the calculation parameters.

The carrier generation rate is considered independent of the spacer layer thickness provided that In content in QW is the same for all of the structures. The recombination rate as well

as the rate of electron spin relaxation can be derived from experimental dependencies of the PL intensity and polarization decay as has been discussed above. Then we believe that Mn vs hole interaction constants (C and D) as well as hole and Mn spin-relaxation rates weakly depend on the spacer layer thickness. The latter can be confirmed by Ref. [24], in which very weak dependence of Mn-hole interaction on the spacer layer thickness was revealed.

In fact, the parameter that changes most drastically with a decrease of a spacer layer thickness is a resident electron concentration in the quantum well [$N_{1,2}^e(0)$]. Indeed, this concentration should decrease upon shifting the QW towards acceptor-type $\delta\langle$Mn$\rangle$ layer. In addition, the variation of $N_{1,2}^e(0)$ is a cornerstone of the qualitative model presented in Fig. 6. We believe that small changes of the equation constant bring insignificant contribution into the ΔP variation as compared with the change of $N_{1,2}^e(0)$. With respect to above considerations, we have chosen the same fitting parameters for all investigated samples with the only exception for resident electron concentration. As a result, the Mn-hole spin-interaction dependence on the distance d is included in our model via the resident electron's concentration scaling function (5).

The results of simulations are presented in Fig. 3 (thick lines) and Fig. 7. Let us first discuss Fig. 7, which shows the time evolution of Mn spin polarization in case of pumping with same polarization and opposite polarization of pulses. One can see that indeed pumping the electron-hole system in the QW leads to high polarization of Mn due to the interaction terms C and D [see Eq. (3)]. Figure 7(a) shows the unbalance between two Mn spin states after excitation with the pump pulse. We also note a significant asymmetry between the cases of same and opposite polarizations. In the first case the probe pulse only slightly increases the polarization since the Mn subsystem is already polarized by the pump pulse; see Fig. 7(a). For the second case, in contrast, the probe pulse switches the Mn polarization to the opposite direction, almost close to zero (difference between two Mn spin states), Fig. 7(b). In the case of Mn spin-reversal Mn-hole interaction makes smaller contribution to the resulting polarization of the PL after the probe pulse, which is confirmed by the experiment. Thus, hole spin polarization is indeed influenced by the *Mn* layer working opposite to probe-pulse polarization.

Since *Mn* spins are subject to spin relaxation on the characteristic time $\tau_{Mn} = 1/\gamma_{Mn}$, one can expect a decrease of the spin-memory effect when the window between the pulses is extended and the *Mn* spin system loses some of its polarization before the second pulse arrives.
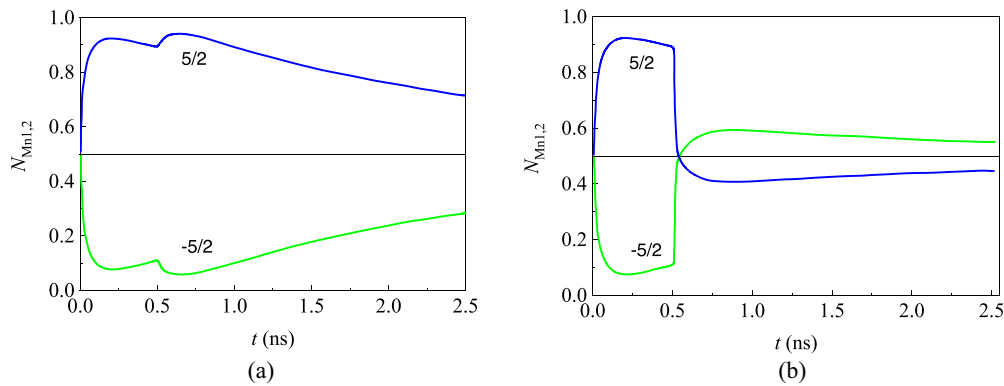
FIG. 7. The calculated time dependence of concentration of Mn atoms in $\delta\langle$Mn$\rangle$ layer having the polarization of 5/2 and $-5/2$ upon the excitation of electron-hole subsystem by the pulses of σ^+-σ^+ excitation sequence (a) and σ^+-σ^- excitation sequence (b).

The Mn spin-relaxation time used in calculations and derived from the experiment for the investigated sample ($1/\gamma_{Mn} = 5$ ns) is by an order or even two orders of magnitude greater than the ones reported in a majority of experiment papers on (Ga,Mn)As layers with close Mn content [25–30]. However, we should note that the magnetic impurity structure of the investigated system differs from the ones reported in Refs. [25–30]. Unlike the uniformly doped (Ga,Mn)As structures [25–30], the Mn content for our case is nonuniform Gauss-like function of the depth with the maximum at the distance ds from quantum well [31]. At the vicinity of the quantum well Mn content is consistent with the GaAs:Mn layer investigated in Ref. [30] for which $1/\gamma_{\mathrm{Mn}}$ values of the order of 5 ns were also reported.

The reason for such spin-relaxation time decrease is believed to be a strong suppression of spin-relaxation mechanism associated with spin-orbit coupling (such mechanism was discussed in Refs. [26,27]). The latter occurs due to a low concentration of holes localized in $\delta\langle$Mn$\rangle$ layer ($\sim$0.1 of Mn content as reported in Ref. [31]), which is caused by the compensation of holes by Mn interstitials in GaAs. We believe that such lack of the holes both determines lower Curie temperature as compared with Refs. [25–29] and makes one of the Mn spin-relaxation mechanisms inefficient.

Figure 4 (thick curves) clearly shows the dependence of calculated ΔP on the time delay between two pulses. This dependence is in satisfactory agreement with the experimental ones (compare dots and thick lines in Fig. 4) with the only exception for sample No. 4. Despite some quantitative disagreement one can state that the model of the photoluminescence kinetics (3) when correctly applied reflects the trends of the investigated system behavior discussed above. First, with the increase of Δt the ΔP value decreases. The extracted relaxation time for *Mn* spins is about 5 ns, which agrees with previous experiment results [13,14]. Second, the decrease of resident electron concentration leads to decrease of spin-memory effect, as observed for samples with different d. As a final note we should mention that our model takes into account the presence of pump-generated carriers in the QW at the moment of probe-pulse arrival in case of short Δt values. For that reason, the calculated values of ΔP include contribution from both Mn-affected polarization and pump-pulse polarization. In order to exclude the second factor in the

first approximation one is to subtract the exponential decay of pump PL intensity from the PL intensity of the second pulse. Such procedure was performed for the experimental data; the results are shown in Fig. 2 as open dots.

V. CONCLUSIONS

We have investigated the spin-memory effect in the GaAs/InGaAs quantum wells with $\delta\langle$Mn$\rangle$ layer in GaAs barrier. The effect consists of spin polarization of Mn atoms due to interaction with photogenerated spin-polarized holes. The investigation of the effect was carried out by analyzing the polarization of the probe photoluminescence pulse in the pump-probe technique. It was shown that the circular polarization degree of probe-pulse generated photoluminescence is strongly affected by the interaction of hole spins with spins of Mn atoms polarized by the pump pulse. The latter leads to decrease of circular polarization degree as compared with single-pulse excitation (quantified by the residual polarization, so-called ΔP effect). The amplitude of ΔP effect is most strongly affected by the concentration of resident electrons in the quantum well, which is believed to be due to the specific compliance with selection rules for optical transition with the participation of unpolarized resident electrons. The rest of the sample's parameters including the spatial separation between $\delta\langle$Mn$\rangle$ layer and InGaAs quantum well (d_s) have a minor effect on the ΔP value which leads to a paradoxical situation of decreasing ΔP-effect with the decrease of d_s. The proposed experimental technique consisting of creating the significant concentration of resident electrons in the QW may serve as a reliable photoluminescence method determining the strength of this effect as well as the *Mn* spin-relaxation time in a particular nanostructure.

[1] D. K. Young, J. A. Gupta, E. Johnston-Halperin, R. Epstein, Y. Kato, and D. D. Awschalom, Semicond. Sci. Technol. **17**, 275 (2002).

[2] M. Holub and P. Bhattacharya, J. Phys. D: Appl. Phys. **40**, R179 (2007).

[3] T. Jungwirth, J. Wunderlich, V. Novák, K. Olejník, B. L. Gallagher, R. P. Campion, K. W. Edmonds, A. W. Rushforth, A. J. Ferguson, and P. Němec, Rev. Mod. Phys. **86**, 855 (2014).

[4] A. Hirohata, K. Yamada, and Y. Nakatani, J. Magn. Magn. Mater. **509**, 166711 (2020).

[5] R. C. Myers, A. C. Gossard, and D. D. Awschalom, Phys. Rev. B **69**, 161305(R) (2004).

[6] A. M. Nazmul, T. Amemiya, Y. Shuto, S. Sugahara, and M. Tanaka, Phys. Rev. Lett. **95**, 017201 (2005).

[7] M. V. Dorokhin, Yu. A. Danilov, P. B. Demina, V. D. Kulakovskii, O. V. Vikhrova, S. V. Zaitsev, and B. N. Zvonkov, J. Phys. D: Appl. Phys. **41**, 245110 (2008).

[8] S. V. Zaitsev, V. D. Kulakovskii, M. V. Dorokhin, Yu. A. Danilov, P. B. Demina, M. V. Sapozhnikov, O. V. Vikhrova, and B. N. Zvonkov, Physica E **41**, 652 (2009).

[9] V. I. Korenev, I. A. Akimov, S. V. Zaitsev, V. F. Sapega, L. Langer, D. R. Yakovlev, Yu. A. Danilov, and M. Bayer, Nat. Commun. **3**, 959 (2012).

[10] I. A. Akimov, V. L. Korenev, V. F. Sapega, L. Langer, S. V. Zaitsev, Yu. A. Danilov, D. R. Yakovlev, and M. Bayer, Phys. Status Solidi B **251**, 1663 (2014).

[11] M. A. G. Balanta, M. J. S. P. Brasil, F. Iikawa, J. A. Brum, U. C. Mendes, Yu. A. Danilov, M. V. Dorokhin, O. V. Vikhrova, and B. N. Zvonkov, J. Appl. Phys. **116**, 203501 (2014).

[12] M. V. Dorokhin, Yu. A. Danilov, B. N. Zvonkov, M. A. G. Balanta, M. J. S. P. Brasil, F. Iikawa, U. C. Mendes, J. A. Brum, P. B. Demina, E. I. Malysheva, A. V. Zdoroveyshchev, and A. V. Kudrin, Appl. Phys. Lett. **107**, 042406 (2015).

[13] M. A. G. Balanta, M. J. S. P. Brasil, F. Iikawa, U. C. Mendes, J. A. Brum, Yu. A. Danilov, M. V. Dorokhin, O. V. Vikhrova, and B. N. Zvonkov, Sci. Rep. **6**, 24537 (2016).

[14] F. C. D. Moraes, S. Ullah, M. A. G. Balanta, F. Iikawa, Y. A. Danilov, M. V. Dorokhin, O. V. Vikhrova, B. N. Zvonkov, and F. G. G. Hernandez, Sci. Rep. **9**, 7294 (2019).

[15] M. Dyakonov and V. Perel, in *Modern Problems in Condensed Matter Sciences*, edited by F. Meier and B. P. Zakharchenya, Optical Orientation Vol. 8 (Elsevier, Amsterdam, 1984).

[16] Yu. N. Drozdov, N. V. Baidus', B. N. Zvonkov, M. N. Drozdov, O. I. Khrykin, and V. I. Shashkin, Semiconductors **37**, 194 (2003).

[17] D. V. Yurasov and Yu. N. Drozdov, Semiconductors **42**, 563 (2008).

[18] J. Mickevicius, G. Tamulaitis, E. Kuokstis, M. S. Shur, J. Yang, and R. Gaska, Acta Phys. Pol. A **114**, 1247 (2008).

[19] L. Lu, J. Wang, Y. Wang, W. Geb, G. Yang, and Z. Wang, J. Appl. Phys. **83**, 2093 (1998).

[20] M. M. Glazov, *Electron and Nuclear Spin Dynamics in Semiconductor Nanostructures* (Oxford University Press, Oxford, 2018).

[21] J. Hubner and M. Oestreich, Semicond. Sci. Technol. **23**, 114006 (2008).

[22] T. S. Shamirzaev, J. Debus, D. R. Yakovlev, M. M. Glazov, E. L. Ivchenko, and M. Bayer, Phys. Rev. B **94**, 045411 (2016).

[23] T. S. Shamirzaev, J. Rautert, D. R. Yakovlev, J. Debus, A. Yu. Gornov, M. M. Glazov, E. L. Ivchenko, and M. Bayer, Phys. Rev. B **96**, 035302 (2017).

[24] M. V. Dorokhin, P. B. Demina, E. I. Malysheva, A. V. Kudrin, M. V. Ved' and A. V. Zdoroveyshchev, Tech. Phys. Lett. **46**, 87 (2020).

[25] I. A. Akimov, G. V. Astakhov, R. I. Dzhioev, K. V. Kavokin, V. I. Korenev, Yu. G. Kusrayev, D. R. Yakovlev, M. Bayer, and L. W. Molenkamp, Solid State Phenom. **168-169**, 47 (2011).

[26] I. V. Krainov, V. F. Sapega, N. S. Averkiev, G. S. Dimitriev, K. H. Ploog, and E. Lähderanta, Phys. Rev. B **92**, 245201 (2015).

[27] I. V. Krainov, N. S. Averkiev, and E. Lähderanta, Low Temp. Phys. **43**, 449 (2017).

[28] A. V. Scherbakov, A. S. Salasyuk, A. V. Akimov, X. Liu, M. Bombeck, C. Bruggemann, D. R. Yakovlev, V. F. Sapega, J. K. Furdyna, and M. Bayer, Phys. Rev. Lett. **105**, 117204 (2010).

[29] Y. Zhu, X. Zhang, T. Li, L. Chen, J. Lu, and J. Zhao, Appl. Phys. Lett. **94**, 142109 (2009).

[30] R. C. Myers, M. H. Mikkelsen, J.-M. Tang, A. C. Gossard, M. E. Flatte, and D. D. Awschalom, Nat. Mater. **7**, 203 (2008).

[31] Yu. A. Danilov, M. N. Drozdov, Yu. N. Drozdov, A. V. Kudrin, O. V. Vikhrova, B. N. Zvonkov, I. L. Kalentieva, and V. S. Dunaev, J. Spintron. Magn. Nanomater. **1**, 82 (2012).